Energy & Environmental Science

Exceptional Thermoelectric Performance in $Mg_3Sb_{0.3}Bi_{1.4}$ for low-grade waste heat recovery

Journal:	*Energy & Environmental Science*
Manuscript ID	EE-COM-11-2018-003374.R2
Article Type:	Communication
Date Submitted by the Author:	31-Jan-2019
Complete List of Authors:	Imasato, Kazuki; Northwestern University, Kang, Stephen; California Institute of Technology, ; Northwestern University, Snyder, G.; Northwestern University, Materials Science

Exceptional Thermoelectric Performance in $Mg_3Sb_{0.6}Bi_{1.4}$ for low-grade waste heat recovery

Kazuki Imasato[1], Stephen Dongmin Kang*[1,2] and G. Jeffrey Snyder†[1]

[1]*Northwestern University, Evanston, IL 60208, USA,* [2]*California Institute of Technology, Pasadena, CA 91125, USA*

Bi_2Te_3 alloys have been the most widely used n-type material for low temperature thermoelectric power generation for over 50 years, thanks to the highest efficiency in the 300 − 500 K temperature range relevant for low-grade waste-heat recovery. Here we show that n-type $Mg_3Sb_{0.6}Bi_{1.4}$, with a thermoelectric figure-of-merit zT of 1.0-1.2 at 400-500 K, finally surpasses n-type Bi_2Te_3. This exceptional performance is achieved by tuning the alloy composition of $Mg_3(Sb_{1-x}Bi_x)_2$. The two primary mechanisms of the improvement are the band effective-mass reduction and grain size enhancement as the Mg_3Bi_2 content increases. The benefit of the effective-mass reduction is only effective up to the optimum composition $Mg_3Sb_{0.6}Bi_{1.4}$, after which a different band dominates charge transport. The larger grains are important for minimizing grain-boundary electrical resistance. Considering the limited choice for low temperature n-type thermoelectric materials, the development of $Mg_3Sb_{0.6}Bi_{1.4}$ is a significant advancement towards sustainable heat recovery technology.

Broader Context

One of the bottlenecks for low-grade waste-heat recovery using thermoelectrics is the lack of a good n-type material that performs well around 400-500 K. For more than 50 years, n-type Bi_2Te_3 has been the standard material for this application, and the field has not seen any superior alternatives. Having only one material option can also greatly limit the device design space that one could utilize. When designing thermoelectric devices, many more properties other than just the maximum performance can be restricting factors: cost and availability of the material; chemical stability when interfaced with other materials; mechanical reliability; thermal shock resistance; thermoelectric compatibility for segmenting. With the demonstration of n-type $Mg_3Sb_{0.6}Bi_{1.4}$ with properties offering higher energy conversion efficiency than Bi_2Te_3 for low-grade waste-heat recovery, the material could become a next-generation material for low temperature thermoelectrics.

Globally, more than half of the energy in fuels is lost as waste heat to the environment. Strategies for converting this wasted energy into a useful form like electricity depends on the temperature of the waste heat. In particular, low-grade waste heat (temperatures lower than 250°C) offers a great opportunity because of its huge portion amounting to 300 TBtu/yr of work potential[1]. Thermoelectric generation is one of the most promising technologies for recovering this low-grade waste heat and solving today's energy challenges[2,3].

The maximum energy conversion efficiency of a thermoelectric material is assessed by using the dimensionless figure-of-merit zT, defined as $zT = S^2\sigma T/\kappa$ where S is the Seebeck coefficient, σ is the electrical conductivity, κ is the thermal conductivity, and T is the temperature. An average zT value near unity in the temperature range of use is typically needed to make thermoelectric conversion a useful process.

*Stephen.D.Kang@gmail.com

†Jeff.Snyder@northwestern.edu

In the temperature range for low-grade waste heat recovery (below 250°C), there are few high performance thermoelectric materials, especially on the n-type side. Currently, Bi_2Te_3 and its related compounds are the only practical n-type materials in this temperature range (typically exhibiting $zT \approx 1$ at 400 K), a material that dates back to 1954[4,5]. The situation is in contrast to p-type materials where Bi_2Te_3 has higher zT values (when nano-engineered[6,7]) and also other potentially good materials exist[3].

The Mg_3Sb_2-Mg_3Bi_2 alloy is one of the few high performance n-type materials, recently discovered[8,9] and originally optimized for its mid-temperature (above 500 K) application with the specific composition $Mg_{3+\delta}Sb_{1.5}Bi_{0.5}Te_{0.01}$ ($zT \approx 1.5$ at 700 K)[10]. Alloying with Mg_3Bi_2 reduces the thermal conductivity[8,11], but also significantly changes the electrical band structure[12]. The alloying effect on bands implies that one should be able to tune this material for low temperatures by employing band engineering strategies.

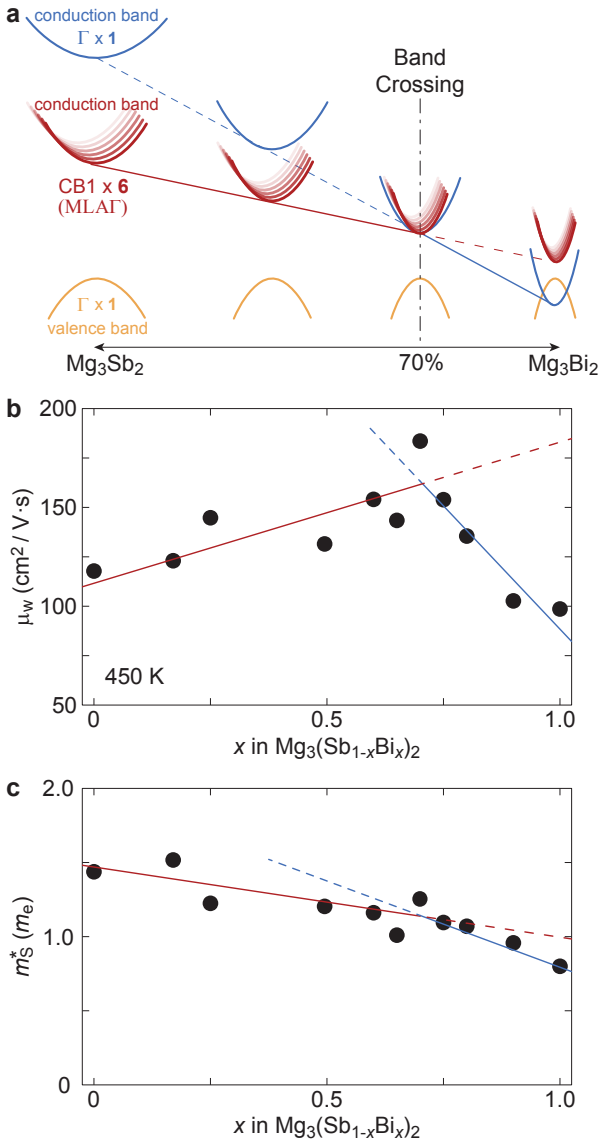

Figure 1: Conduction band optimization in the solid solution of Mg_3Sb_2-Mg_3Bi_2 for low-temperature thermoelectrics. a Schematic of how the relative energy of bands change with alloying. The effective mass of all bands reduces with increasing Mg_3Bi_2 content in the solid solution. The single-valley Γ band (blue) crosses over the six-fold valley conduction band CB1 (red), eventually circumventing the multi-valley benefit of CB1. The optimum band structure is obtained near the conduction band crossing, when the effective mass is minimized while maintaining valley degeneracy. **b** Weighted mobility of the conduction band at 450 K shows a maximum peak around 70 % alloying ($Mg_3Sb_{0.6}Bi_{1.4}$). **c** The Seebeck effective mass of the conduction band decreases with Mg_3Bi_2 alloying because of the increased curvature of the bands. Since a lighter band mass is favorable for mobility, the optimum thermoelectric composition is where the six-fold CB1 band is lighter but still the lowest conduction band. The lack of a noticeable peak in m_S^* at 70 % indicates that the convergence effect is minimal. The lines in **b** and **c** are guides to the eyes.

Band Engineering Strategy

The goal of band engineering in thermoelectrics is to increase the weighted mobility μ_w, which is the electronic part of the material quality factor[13,14] B:

$$B \propto \frac{\mu_w}{\kappa_L} \propto \frac{N_V}{m_I^* \kappa_L}. \quad (1)$$

Here, κ_L is lattice thermal conductivity, N_V is valley degeneracy, and m_I^* is inertial effective mass of the charge carriers. Since a higher maximum zT is obtainable with higher B, maximizing μ_w is desired, which can be achieved through either increasing N_V or reducing m_I^*. The typical band engineering strategy is to converge multiple bands to have the same band edge[15–17], which effectively increases N_V. A different strategy often overlooked is to reduce m_I^*. The conduction bands of Mg_3Sb_2 can be made lighter by alloying with Mg_3Bi_2, which has the same band structure but with bands that have more curvature and therefore have lighter charge carriers (smaller m_I^*) [12].

Decreasing the conduction band mass by increasing the Mg_3Bi_2 content of Mg_3Sb_2-Mg_3Bi_2 alloys should increase μ_w and therefore zT. Increasing the Mg_3Bi_2 content also shrinks the band gap (Fig.1a) and brings the peak in zT with respect to T to a lower temperature[12]. Although a narrow gap is not usually desired as the thermally excited bipolar conduction (by holes and electrons) effectively limits the maximum operation temperature, the benefit of the reduced band mass for use at lower temperature can outweigh the disadvantage of a more limited operation temperature.

The benefit of increasing the Mg_3Bi_2 content should only be effective up to an optimum composition due to the band crossing of the conduction bands. According to band structure calculations[18,19], the lowest conduction band in Mg_3Bi_2 is the single-valley Γ band rather than the six-valley MLAΓ band (CB1). Thus, one can expect a band crossing to occur in Mg_3Sb_2-Mg_3Bi_2 alloys when the Mg_3Bi_2 content is high, at about 70 % of Mg_3Bi_2 (see Fig.1a). Once the Γ band becomes the lowest and dominant conduction band, the effective valley degeneracy is reduced and the band gap rapidly decreases, which will lead to detrimental bipolar conduction. Therefore, the optimum composition is expected to be around 70 % of Mg_3Bi_2, or $Mg_3Sb_{0.6}Bi_{1.4}$, which is the composition with maximum Mg_3Bi_2 content before the band crossing. Regardless of whether the Γ band makes a meaningful contribution at the band crossing composition, highest thermoelectric performance is expected at this alloy composition due to the decreased band mass of CB1. The n-type Goldsmid-Sharp band gap (the effective band gap for transport) at the band crossing composition $Mg_3Sb_{0.6}Bi_{1.4}$ is 0.2 eV, which is still suitable for applications below 500 K (the true gap is smaller[12]; see ESI).

Results

Optimum Composition from Weighted Mobility

To experimentally identify the composition at which the electronic transport properties are optimal, the weighted mobilities, μ_w, are determined from the measured electrical conductivity and Seebeck coefficient values (see Methods). Weighted mobility is a Fermi-level independent quantity that is most directly relevant in determining the conductivity one can get from a given Seebeck coefficient[13,14]. It is the most useful form for this analysis because, in principle, it does not change strongly with doping concentration like Seebeck or conductivity does. Fig.1b shows the weighted mobilities of the n-type charge carriers in $Mg_3(Sb_{1-x}Bi_x)_2$.

A maximum in the μ_w (T = 450 K) is found at a composition of 70 % Mg_3Bi_2 (Fig.1b), consistent with the expected band engineering strategy. The increase in μ_w (red line) with Mg_3Bi_2 content up to the maximum at 70 % Mg_3Bi_2 is attributed primarily to the reduction in m_I^* (Eq.1). The abrupt change to a decreasing trend (blue line) is attributed to the band crossover, which reduces the effective N_V as the singly degenerate conduction band at Γ becomes increasingly more dominant. Therefore, the optimum electronic structure found by transport measurements coincides with the composition $Mg_3Sb_{0.6}Bi_{1.4}$.

Furthermore, the change in the Seebeck effective mass[12,13] (m_S^*, which is a density-of-states mass that depends on both N_V and band curvature) also supports the understanding of band structure optimization. The decrease in m_S^* with alloying (Fig.1c, red line) is due to the curvature increase of the CB1 bands. One can also notice that the kink in the m_S^* trend at the band crossover is not as pronounced because of the strong remaining influence of CB1. This subtlety indicates that the band convergence effect is minimal as expected from the small valley degeneracy of the Γ band. Even after the crossing, the CB1 bands still contribute to the Seebeck coefficient because of the much higher valley degeneracy (×6) and small energy offset from the Γ band.

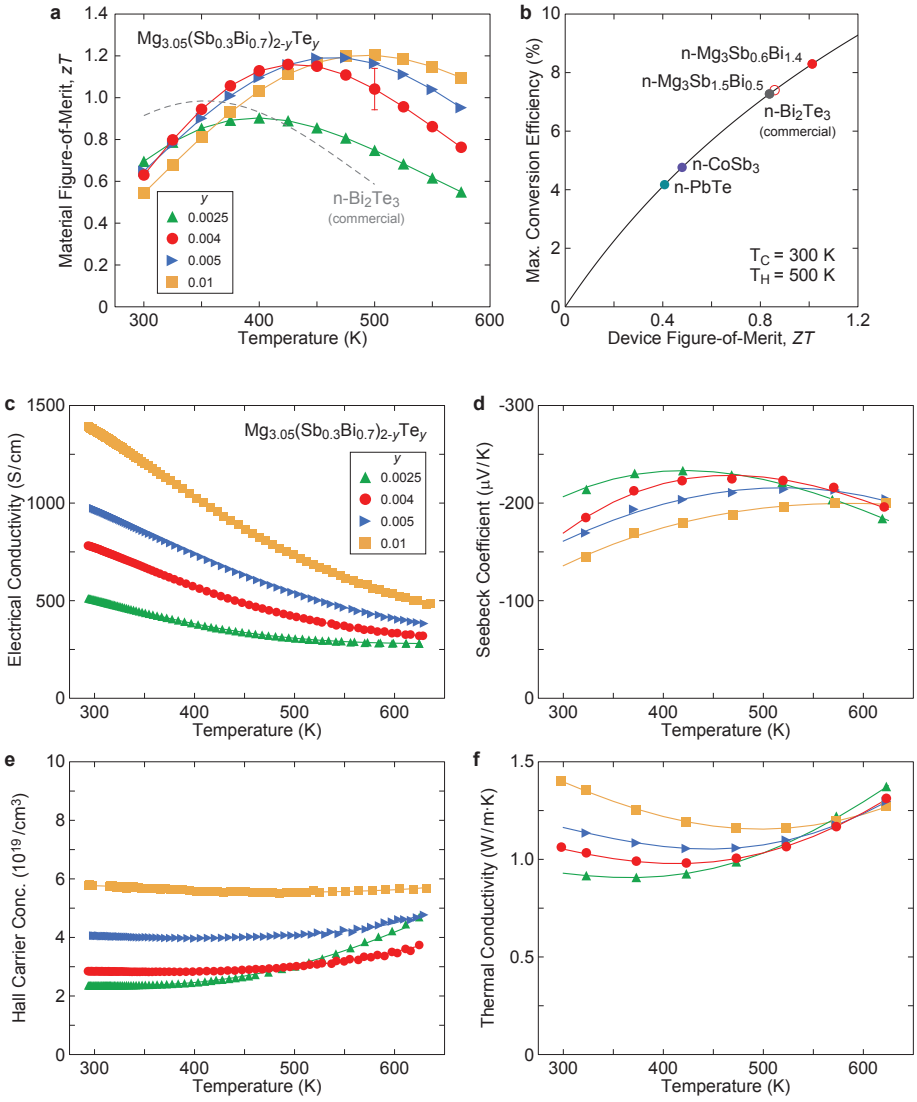

Figure 2: Thermoelectric performance in n-type $Mg_3Sb_{0.6}Bi_{1.4}$ for low-grade waste-heat recovery exceeding that of standard n-type materials. a The material figure-of-merit with various n-type doping levels, compared with the current commercial material n-type Bi_2Te_3. Nominal compositions are indicated in the legend. The error bar represents an estimated standard deviation including variations in Seebeck, resistance, and thickness measurements. **b** The maximum conversion efficiency obtainable with a 500 K hot-side leg-temperature and room temperature cold-side leg-temperature. An efficiency of > 8 % is possible with the best composition. The efficiencies were calculated from individual transport properties and by considering self-compatibility[20] (see SI). **c** Electrical conductivity, **d** Seebeck coefficient, **e** Hall carrier concentration (inverse of the Hall coefficient), and **f** Thermal conductivity of $Mg_3Sb_{0.6}Bi_{1.4}$ doped with various amounts of Te on the anion site. Reference data from: [21] (Bi_2Te_3); [22] ($CoSb_3$); [23, 24] (PbTe); [10] ($Mg_3Sb_{1.5}Bi_{0.5}$).

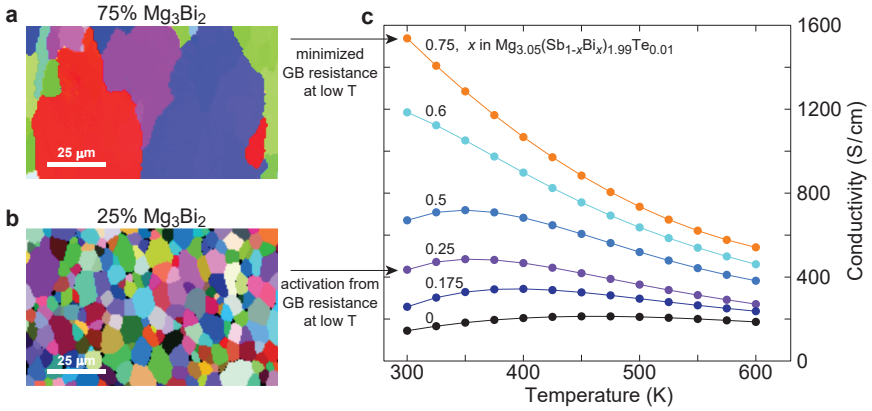

Figure 3: Minimized grain boundary resistance with high Mg_3Bi_2 content. a,b The grain size observed with electron back-scattering diffraction in alloyed pellet samples with 75 % (a) and 25 % (b) Mg_3Bi_2 content. The average grain size in the 75 % sample is 5-10 times larger than that of 25 % due to increased grain-growth kinetics. **c** Temperature-dependent conductivity with varied Mg_3Bi_2 content in the alloy. The effect of grain boundary resistance is seen by the activated conductivity near room temperature, which is pronounced in the small grain sample but not apparent in the large grain sample. The increase in the *magnitude* of conductivity with respect to Mg_3Bi_2 content is due to both an increase in μ_w and a reduction in grain boundary resistance. All samples shown were consolidated with identical conditions (see Methods).

Thermoelectric performance at the optimal composition $Mg_3Sb_{0.6}Bi_{1.4}$

The optimal composition $Mg_3Sb_{0.6}Bi_{1.4}$ indeed shows excellent low-temperature thermoelectric performance, much better than standard n-type materials (Fig.2). By varying the doping concentration of $Mg_3Sb_{0.6}Bi_{1.4}$ where best μ_w was found, we find zT values higher than unity in the range of 350-600 K, a significant improvement compared with the commercial n-type Bi_2Te_3 material (Fig.2a). The maximum obtainable energy conversion efficiency exceeds 8 % for a thermoelectric leg at 300 and 500 K at each side, corresponding to a device figure-of-merit[20] $ZT > 1$ (Fig.1b), also higher than both the commercial n-type Bi_2Te_3 and the $Mg_3Sb_{1.5}Bi_{0.5}$ composition previously optimized for mid-temperature. The detailed nominal composition of the sample with highest conversion efficiency was $Mg_{3.05}(Sb_{0.3}Bi_{0.7})_{1.996}Te_{0.004}$ (red circles in Fig.1). Here, excess Mg ($3 + \delta$ in the formula) is required to ensure the stable acquirement of n-type properties[25], but is minimized to not increase thermal conductivity[26]. Te is the n-type dopant that provides the optimum carrier concentration. The individual transport properties are shown in Fig.2c-f.

Mitigation of Grain Boundary Resistance

A critical prerequisite for fully taking advantage of the benefits from band engineering in this material is the minimization of grain boundary resistance. It has been shown in recent studies[10,27] that the grain boundary resistance is the reason for low and thermally activated conduction below 500 K (rather than ionized impurity scattering). This grain boundary resistance leads to poor thermoelectric performance at low-grade waste-heat temperatures, which is one reason why the material was not seriously considered for low temperatures in previous investigations. An effective solution for such a material is to maximize the grain size and thereby minimize the grain boundary density.

Increasing the Mg_3Bi_2 content greatly enhances the grain growth kinetics, allowing the samples to have larger grains and minimal grain boundary resistance. Electron microscopy of the 75 and 25 % Mg_3Bi_2 samples shows a 5-10 times grain size difference (Fig.3a-b) when prepared under identical conditions (consolidated at 800°C for 20 min to limit Mg loss[25,28]). The thermally-activated behavior in the low temperature electrical conductivity (Fig.3c) is substantially removed with larger grains. This microstructure enables the material to take full advantage of the band structure optimized for low temperature. Enhanced grain growth kinetics can be expected from the decreasing melting temperature as the Mg_3Bi_2 content increases (Mg_3Bi_2 melts at 820°C while Mg_3Sb_2 melts at 1120°C). We note that, the increase in grain size does not compromise the low thermal conductivity in this material due to the inherently short mean free paths of phonons[10,29,30], unlike other materials such as Bi_2Te_3 where grain size reduction is a useful strategy[7].

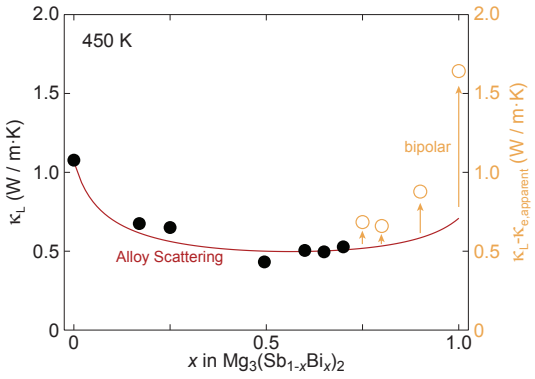

Figure 4: Phonon scattering from Sb-Bi disorder. Lattice thermal conductivity (solid circles) as a function of alloy composition, consistent with the behavior expected from the alloy scattering model (red solid line, see ESI). Near the optimum composition ($x = 0.7$), lattice thermal conductivity is insensitive to the composition and is similar to the minimum found at $x = 0.5$. Near the Mg_3Bi_2 composition, the bipolar effect is pronounced giving significantly higher thermal conductivity values. Open circles represent values obtained by treating the transport properties as if there were no minority carrier contributions (an apparent subtraction of the electronic contribution). The disparity from the alloy scattering curve is indicative of pronounced bipolar thermal conductivity. Data points were extracted from samples with nominal compositions of $Mg_{3.05}(Sb_{1-x}Bi_x)_{1.99}Te_{0.01}$.

Thermal conductivity

Alloying has a beneficial effect also for reducing thermal conductivity (Fig.4) because the Sb-Bi disorder helps to scatter phonons; however, near the electronic optimal composition (70 % Mg_3Bi_2), the lattice thermal conductivity is not very sensitive to the composition (consistent with the alloy scattering model). Therefore, in terms of finding the optimum composition, the electronic consideration on μ_w is much more important than controlling the thermal conductivity. The quality factor evaluation is discussed in the ESI.

Conclusions

To summarize, the band structure of $Mg_3(Sb_{1-x}Bi_x)_2$ can be tuned such that the thermoelectric performance is optimized for low-grade waste-heat temperatures. The primary benefit comes from the decrease in the band mass of the six-valley conduction band as the Mg_3Bi_2 content is increased. This benefit is maximum at the band crossing point, beyond which the single-valley Γ band becomes the lowest conduction band. Bipolar conduction at the band-crossing composition is not as severe as what the true band gap might suggest, thanks to the large contrast between n-type and p-type weighted mobilities that gives a larger effective gap for n-type $Mg_3(Sb_{1-x}Bi_x)_2$.

Methods

Weighted Mobility Analysis

To determine the weighted mobilities from the measured electrical conductivity and Seebeck coefficient data, it is important to obtain values representing the intrinsic properties of the majority carriers. From the raw measurement data, we identify temperature regions that are not affected by bipolar conduction (which would reduce the extracted μ_w to below the intrinsic value). Furthermore, we also exclude regions where grain boundary resistance is significant. Use of the remaining regions ensures the values obtained are closest to the intrinsic μ_w values (See ESI for details of the analysis procedure and also the raw data). It should be noted that an energy dependency of $E^{-1/2}$ for scattering time, rather than $E^{3/2}$, should be used for the analysis. It has been shown[27] through the $\log|S| - \log\sigma$ analysis[31,32] that such energy dependency is indeed the case at and above room temperature, as opposed to some earlier suggestions about ionized impurity scattering[33].

Sample Synthesis

Samples with nominal compositions of $Mg_{3.05}(Sb_{1-x}Bi_x)_{1.99}Te_{0.01}$ (x = 0 to 1.0) and $Mg_{3.05}(Sb_{0.3}Bi_{0.7})_{2-y}Te_y$ (y = 0.0025 to 0.01) were synthesized. Weighed magnesium turnings (99.98%, metals basis, Alfa Aesar), antimony shots (99.9999%, metals basis, Alfa Aesar), bismuth granules (99.997%, metals basis, Alfa Aesar), and tellurium lumps (99.999%, metals basis, Alfa Aesar) were loaded into stainless steel vials together with stainless steel balls. All weighing and loading were done inside an argon-filled glove box. Elements were reacted by mechanical alloying with a shaker (SPEX 8000D) for two hours. The product powder was extracted from the vial and loaded into a carbon die, in which the powder was consolidated into pellets by rapid hot pressing[34] with 45 MPa at 1073 K for 20 min, under dynamic argon atmosphere.

Property Characterization

The Seebeck coefficients were measured under high vacuum by a two-probe configuration with Chromel/Nb thermocouples embedded in heater blocks to prevent cold finger effects[35]. The Hall coefficients and electrical conductivities were measured under high vacuum by using the four-probe van der Pauw method with Mo probes and a 2 T electromagnet[24]. Thermal diffusivities were measured by using the laser flash method (Netzsch LFA 457) under dynamic argon atmosphere. Pellet densities were measured with the geometric method. Heat capacity values based on experimental measurements (see SI or Ref.[36]) were used to calculate thermal conductivities from diffusivity measurements. Electron backscattering diffraction maps were obtained using a scanning electron microscope (Quanta 650 FEG) equipped with a detector (Oxford Instruments Nordlys).

Author Contributions

KI synthesized and measured the samples. KI and SDK analyzed the data. SDK and KI wrote the manuscript. SDK supervised the project with the advice from GJS. All authors reviewed or edited the manuscript.

Acknowledgments

The authors would like to acknowledge support from the NASA Science Mission Directorate's Radioisotope Power Systems Thermoelectric Technology Development program. KI acknowledges support from the Funai Foundation for Information Technology. The EBSD in this work made use of the EPIC facility of Northwestern University's NUANCE Center, which has received support from: the Soft and Hybrid Nanotechnology Experimental Resource (NSF ECCS-1542205); the MRSEC program (NSF DMR-1720139) at the Materials Research Center; the International Institute for Nanotechnology (IIN); the Keck Foundation; the State of Illinois, through the IIN.

Competing interests

The authors declare no competing interests.

References

1. BCS, Incorporated. Waste Heat Recovery: Technology and Opportunities in U.S. Industry. *(United States Department of Energy, Office of Energy Efficiency and Renewable Energy)* (2008).
2. Bell, L. E. Cooling, Heating, Generating Power, and Recovering Waste Heat with Thermoelectric Systems. *Science* **321,** 1457–1461 (2008).
3. Snyder, G. J. & Toberer, E. S. Complex thermoelectric materials. *Nature Materials* **7,** 105–114 (2008).
4. Goldsmid, H. J. & Douglas, R. W. The use of semiconductors in thermoelectric refrigeration. *British Journal of Applied Physics* **5,** 386–390 (1954).

5. Goldsmid, H. J. XXVII. Thermoelectric Applications of Semiconductors. *Journal of Electronics and Control* **1,** 218–222 (1955).
6. Kim, S. I. *et al.* Dense dislocation arrays embedded in grain boundaries for high-performance bulk thermoelectrics. *Science* **348,** 109–114 (2015).
7. Poudel, B. *et al.* High-Thermoelectric Performance of Nanostructured Bismuth Antimony Telluride Bulk Alloys. *Science* **320,** 634–638 (2008).
8. Tamaki, H., Sato, H. K. & Kanno, T. Isotropic Conduction Network and Defect Chemistry in $Mg_{3+\delta}Sb_2$-Based Layered Zintl Compounds with High Thermoelectric Performance. *Advanced Materials* **28,** 10182–10187 (2016).
9. Zhang, J. *et al.* Discovery of high-performance low-cost n-type Mg_3Sb_2-based thermoelectric materials with multi-valley conduction bands. *Nature Communications* **8,** 13901 (2017).
10. Kanno, T. *et al.* Enhancement of average thermoelectric figure of merit by increasing the grain-size of $Mg_{3.2}Sb_{1.5}Bi_{0.49}Te_{0.01}$. *Applied Physics Letters* **112,** 033903 (2018).
11. Ponnambalam, V. & Morelli, D. T. On the Thermoelectric Properties of Zintl Compounds $Mg_3Bi_{2-x}Pn_x$ (Pn = P and Sb). *Journal of Electronic Materials* **42,** 1307–1312 (2013).
12. Imasato, K., Kang, S. D., Ohno, S. & Snyder, G. J. Band engineering in Mg_3Sb_2 by alloying with Mg_3Bi_2 for enhanced thermoelectric performance. *Materials Horizons* **5,** 59–64 (2018).
13. Kang, S. D. & Snyder, G. J. Transport property analysis method for thermoelectric materials: material quality factor and the effective mass model. *arXiv:1710.06896 [cond-mat.mtrl-sci].*
14. Zevalkink, A. *et al.* A practical field guide to thermoelectrics: Fundamentals, synthesis, and characterization. *Applied Physics Reviews* **5,** 021303 (2018).
15. Pei, Y. *et al.* Convergence of electronic bands for high performance bulk thermoelectrics. *Nature* **473,** 66–69 (2011).
16. Kim, H.-S. *et al.* High thermoelectric performance in $(Bi_{0.25}Sb_{0.75})_2Te_3$ due to band convergence and improved by carrier concentration control. *Materials Today* **20,** 452–459 (2017).
17. Yang, J. *et al.* On the tuning of electrical and thermal transport in thermoelectrics: an integrated theory–experiment perspective. *npj Computational Materials* **2** (2016).
18. Imai, Y. & Watanabe, A. Electronic structures of Mg_3Pn_2 (Pn=N, P, As, Sb and Bi) and Ca_3N_2 calculated by a first-principle pseudopotential method. *Journal of Materials Science* **41,** 2435–2441 (2006).
19. Petrov, E. K., Silkin, I. V., Koroteev, Y. M. & Chulkov, E. V. Effect of deformation on the electronic structure and topological properties of the $A^{II}Mg_2Bi_2$ (A^{II} = Mg,Ca,Sr,Ba) compounds. *JETP Letters* **105,** 502–507 (2017).
20. Snyder, G. J. & Snyder, A. H. Figure of merit ZT of a thermoelectric device defined from materials properties. *Energy & Environmental Science* **10,** 2280–2283 (2017).
21. Marlow Industries, Private Communication. unpublished.
22. Tang, Y. *et al.* Convergence of multi-valley bands as the electronic origin of high thermoelectric performance in $CoSb_3$ skutterudites. *Nature Materials* **14,** 1223–1228 (2015).
23. LaLonde, A. D., Pei, Y. & Snyder, G. J. Reevaluation of $PbTe_{1-x}I_x$ as high performance n-type thermoelectric material. *Energy & Environmental Science* **4,** 2090 (2011).
24. Borup, K. A. *et al.* Measuring thermoelectric transport properties of materials. *Energy & Environmental Science* **8,** 423–435 (2015).
25. Ohno, S. *et al.* Phase Boundary Mapping to Obtain n-type Mg_3Sb_2-Based Thermoelectrics. *Joule* **2,** 141–154 (2018).
26. Imasato, K., Ohno, S., Kang, S. D. & Snyder, G. J. Improving the thermoelectric performance in $Mg_{3+x}Sb_{1.5}Bi_{0.49}Te_{0.01}$ by reducing excess Mg. *APL Materials* **6,** 016106 (2018).

27. Kuo, J. J. *et al.* Grain boundary dominated charge transport in Mg_3Sb_2-based compounds. *Energy & Environmental Science* **11,** 429–434 (2018).
28. Shuai, J. *et al.* Significant Role of Mg Stoichiometry in Designing High Thermoelectric Performance for $Mg_3(Sb,Bi)_2$-Based n-Type Zintls. *Journal of the American Chemical Society* **140,** 1910–1915 (2018).
29. Peng, W., Petretto, G., Rignanese, G.-M., Hautier, G. & Zevalkink, A. An Unlikely Route to Low Lattice Thermal Conductivity: Small Atoms in a Simple Layered Structure. *Joule* (2018).
30. Xin, J. *et al.* Growth and transport properties of Mg_3X_2 (X =Sb,Bi) single crystals. *Materials Today Physics* **7,** 61–68 (2018).
31. Kang, S. D., Dylla, M. & Snyder, G. J. Thermopower-conductivity relation for distinguishing transport mechanisms: Polaron hopping in CeO_2 and band conduction in $SrTiO_3$. *Physical Review B* **97** (2018).
32. Kang, S. D. & Snyder, G. J. Charge-transport model for conducting polymers. *Nature Materials* **16,** 252–257 (2016).
33. Shuai, J. *et al.* Tuning the carrier scattering mechanism to effectively improve the thermoelectric properties. *Energy & Environmental Science* **10,** 799–807 (2017).
34. LaLonde, A. D., Ikeda, T. & Snyder, G. J. Rapid consolidation of powdered materials by induction hot pressing. *Review of Scientific Instruments* **82,** 025104 (2011).
35. Iwanaga, S., Toberer, E. S., LaLonde, A. & Snyder, G. J. A high temperature apparatus for measurement of the Seebeck coefficient. *Review of Scientific Instruments* **82,** 063905 (2011).
36. Agne, M. T. *et al.* Heat capacity of Mg_3Sb_2, Mg_3Bi_2, and their alloys at high temperature. *Materials Today Physics* **6,** 83–88 (2018).